

Re-initialization-free Level Set Method via Molecular Beam Epitaxy Equation Regularization for Image Segmentation*

Fanghui Song[†], Jiebao Sun[†], Shengzhu Shi[‡], Zhichang Guo[†], and Dazhi Zhang[†]

Abstract. Variational level set method has become a powerful tool in image segmentation due to its ability to handle complex topological changes and maintain continuity and smoothness in the process of evolution. However its evolution process can be unstable, which results in over flattened or over sharpened contours and segmentation failure. To improve the accuracy and stability of evolution, we propose a high-order level set variational segmentation method integrated with molecular beam epitaxy (MBE) equation regularization. This method uses the crystal growth in the MBE process to limit the evolution of the level set function, and thus can avoid the re-initialization in the evolution process and regulate the smoothness of the segmented curve. It also works for noisy images with intensity inhomogeneity, which is a challenge in image segmentation. To solve the variational model, we derive the gradient flow and design scalar auxiliary variable (SAV) scheme coupled with fast Fourier transform (FFT), which can significantly improve the computational efficiency compared with the traditional semi-implicit and semi-explicit scheme. Numerical experiments show that the proposed method can generate smooth segmentation curves, retain fine segmentation targets and obtain robust segmentation results of small objects. Compared to existing level set methods, this model is state-of-the-art in both accuracy and efficiency.

Key words. Image segmentation; The variational level set method; Molecular beam epitaxy equation; Re-initialization free; Scalar auxiliary variable

MSC codes. 54H30, 68U10, 65M06, 65D18

1. Introduction. Image segmentation is an important part of computer vision where the goal is to partition a given image into several regions that usually represent objects of interest. It has attracted significant attention for its wild applications in areas such as medical imaging[7], remote sensing[21], automatic driving robotics[10] and object detection[1].

Numerous image segmentation methods have been developed including thresholding-based models[30], clustering-based models[33], watershed-based models[35], methods with graph theory[40], level set theory[4] and so on[22, 2]. The level set method was initially introduced by Osher and Sethian and has developed into one of the most competitive segmentation methods for its ability to handle complex topological changes [25, 11, 24, 23]. It uses a level set function to describe the difference in image properties between inside and outside the curve and evolve an initial curve into the boundary of the interest object. Compared with other segmentation methods, it has advantages such as no need for parameterization [29], more

*Submitted to the editors DATE:18 July 2023.

Funding: This work was funded by the National Natural Science Foundation of China (12171123, U21B2075, 11971131, 12271130, 11871133), the Natural Science Foundation of Heilongjiang Province (ZD2022A001), the Fundamental Research Funds for the Central Universities(HIT.NSRIF202202, 2022FRFK060020, HIT.NSRIF. 2020081, 2022FRFK060014).

[†]Department of Computational Mathematics, School of Mathematics, Harbin Institute of Technology (21b912024@stu.hit.edu.cn, sunjiebao@hit.edu.cn, mathgzc@hit.edu.cn, zhangdazhi@hit.edu.cn.)

[‡]Corresponding author, Department of Computational Mathematics, School of Mathematics, Harbin Institute of Technology (mathssz@hit.edu.cn).

robustness to noise[42] and more flexibility[7].

One of the most representative level set method is the geodesic active contour (GAC) model [3]. The GAC model is based on the information of the image gradient and distance transformation. It can deal with complex gray distribution and texture but sensitive to the initial position of the curve and has poor segmentation effect on weak boundary objects. Another typical model is the Chan-Vese (CV) model [4]. It is based on the grayscale value and curvature. The CV model can deal with the object segmentation problem of complex shapes, but is applicable only to the image of uniform region. To overcome the challenges posed by inhomogeneous regions, Li *et al.* proposed a region-scalable fitting (RSF) energy model [18], whose fidelity terms are based on local intensity information. This model can handle the segmentation of the inhomogeneous regions. However, this model is also sensitive to the initial curve, often resulting in local minimization and the segmentation results is affected by the image noise severely.

To obtain more accurate and stable segmentation method, it is important to keep the level set function remains as a directed distance function relative to the desired evolving interface, which is called the property of the signed distance function [12]. However, during the evolution process, the level set function usually can not maintain the property of the signed distance function, it may lead to the degeneration of the evolution equation or the unbounded gradients of the level set function, and cause the failure of the segmentation [1]. To overcome this difficulty, one possible approach is to choose the initial counter carefully, i.e. select the signed distance function to an initial given curve surrounding the objects as the initial condition at the initial time [28], and re-initialize the counter such that the curve stays sufficiently smooth and close to the signed distance function [6, 31, 34]. Unfortunately, re-initialization is complex in real implementation and may generate undesirable side effect that can affect the subsequent evolution process and have the risk of preventing new zero curves from emerging, which may lead to undesirable results for image segmentation, such as failures in detecting the interior boundary.

The variational level set method can control the evolution process by adjusting the fidelity and regularization terms. This enables the method to control the evolution speed of the level set function and achieve the expected shape. Thus another approach to keep the signed function property is to limit the evolution process by the regularization term in the framework of variational level set method, which is called re-initialization free method in contrast to re-initialization method.

Estellers *et al* [8] proposed the l^1 optimization model, which minimizing the sum of the absolute values of the differences between the current and updated distance functions at each time step to preserve distance functions. This approach is computationally efficient for using linear programming techniques. Li *et al* developed a series work on re-initialization free method by using the distance regularization term which constrain the gradient of the geometric active curves. They first proposed DR1 regularization term [19] which limits the gradient of the curves to approach 1. It ensures the level set function remains smooth and well-behaved during the evolution process, so as to improve the accuracy and stability of the level set method which is especially important for complex and irregular shapes. But, this method depends on the selection of parameters, such as the regularization parameter and the time step. In addition, it is mainly designed for binary image segmentation and

may not be suitable for other types of problems, such as multi-phase segmentation or shape reconstruction. To address these problems, they further proposed the double-well potential distance regularization term (DR2) [20], which can be easily adapted to handle various types of image segmentation tasks, such as binary, multi-phase, and object tracking. Xie [38] also proposed a regularization term to minimize steep surfaces and smooth the zero level set. This method can deal with the initialization dependency problem that commonly appears in variational level method, but the segmentation results may not be satisfactory for images with a large amount of details. Zhang *et al* summarized the relevant methods of distance regularization and proposed a variation model derived from a reaction-diffusion model [41], which can smooth the evolving curve and prevent it from becoming too jagged or too irregular. Specially, the segmentation process can start from an arbitrary initial curve or surface that is placed inside or outside the object of interest.

In conclusion, the above methods and their variants [17, 22] can avoid re-initialization and improve the accuracy of the segmentation results. However, they may still face challenges in handling complex images with a large amount of details.

Furthermore, the artificial distance regularization term can keep the signed distance property to some distance but lose the advantage of controlling the evolution process by real physical law. Can we improve the segmentation effect by constructing the distance regularization term using the equation with real physical meaning? For this purpose, we propose a high order level set variational segmentation method [26] by using the molecular beam epitaxial (MBE) equation to limit the evolution of the level set function. The MBE is a technique used to deposit thin films of atoms or molecules onto a substrate to create semiconductor devices and other advanced materials. This MBE regularization term we proposed has the following two advantages. First, the nonequilibrium term of the MBE equation forces the gradient of level set function to be 1, which avoids the need for re-initialization. Secondly, the surface diffusion current term, which represents the smoothness constraint of the crystal growth in the MBE process, regulates the smoothness of the segmented curve.

The major contributions of our work are threefold:

- We propose a segmentation method based on the MBE equation. To the best of our knowledge, we are the first to apply MBE to image processing tasks. This idea is reasonable and interesting as MBE is a typical phase-field model with complete physical meaning, which ensures that the evolution process is smooth and controllable, avoiding the problem of insufficiently smooth evolution caused by artificial distance regularization such as DR1 and DR2.
- To overcome the numerical difficulty cause by the high order term, we derive the scalar auxiliary variable (SAV) scheme coupled with the fast Fourier transform (FFT) for the proposed model. The scheme is unconditionally first-order energy stable. Compared with the traditional semi-implicit and semi-explicit finite difference scheme [15], it can improve the computational efficiency significantly, ensuring that the scheme is excellent in both accuracy and efficiency.
- We design various numerical experiments to show the superiorities of the proposed model. The results show that the MBE regularization term can control the range of the gradient of the level set function and obtain more stable evolution process. The segmentation accuracy is independence of initial curve and the MBE model tends to

generate smooth segmentation boundaries and have good anti-noise performance. In addition, the model also works for multi-target and small target image segmentation.

The paper is organized as follows. Section 2 describes our motivation and preliminary knowledge. In section 3, we introduce the MBE regularization term and propose two related models, MBE-GAC and MBE-RSF. In section 4, We design the SAV scheme coupled with FFT method for our model and provide a first-order unconditional energy stability theorem. In section 5, numerical experiments are conducted to illustrate the superiority of the proposed MBE model. Lastly, conclusion is given in section 6.

2. Motivation. Although the level set method has the advantages such as high accuracy, local adaptivities and the ability to handle complex boundaries, its evolution process may be unstable. How to improve the accuracy and stability of the evolution is one of the major challenge in the level set method, which is also the main contribution of this paper. We will demonstrate the detailed motivation of this paper from the aspect of the level set method, the distance regularization term and the property of the molecular beam epitaxial (MBE) equation.

2.1. Level set segmentation method and re-initialization. Let $\Omega \subset \mathbb{R}^2$ be the image domain, $C(t) = (x(t), y(t))$ be a closed curve evolved as follows

$$(2.1) \quad \begin{cases} \frac{\partial C}{\partial t} = \alpha(x, y, t)\mathbf{T} + \beta(x, y, t)\mathbf{N}, & (x, y, t) \in \Omega \times (0, T], \\ C(0) = C_0, & (x, y) \in \Omega, \end{cases}$$

where α is tangential velocity, β is normal velocity, \mathbf{T} and \mathbf{N} represent the unit tangent vector and unit normal vector, respectively, and C_0 is the initial value.

On a local scale, by representing $y = \gamma(x(t), t)$, one has $C(t) = (x(t), \gamma(x, t))$. It follows from $\gamma_t = \frac{dy}{dt} - \gamma_x \frac{dx}{dt} = \beta \sqrt{1 + \gamma_x^2}$ that the evolution of (2.1) can be simplified as

$$(2.2) \quad \frac{\partial C}{\partial t} = \beta \mathbf{N},$$

which shows the change in the geometric shape of a curve only depends on its normal component [1]. Solving (2.2) directly is difficult. To address this issue, Osher and Sethian proposed the level set method [29]. It represent C as a zero level set of a higher dimensional function $\phi : \Omega \rightarrow \mathbb{R}$, which is

$$(2.3) \quad C(t) = \{(x, y) | \phi(x, y, t) = 0\}.$$

In (2.3), $\phi(x, y, t)$ is determined by solving the nonlinear equation,

$$(2.4) \quad \begin{cases} \frac{\partial \phi}{\partial t} = F |\nabla \phi|, & (x, y, t) \in \Omega \times (0, T], \\ \phi(x, y, 0) = \phi_0(x, y), & (x, y) \in \Omega, \end{cases}$$

where $\nabla \phi$ denotes the spatial gradient of ϕ , F is related to normal component of the velocity, which does not change sign during the evolution and the orientation depends on the type of

evolution (outward for an expansion and inward for a shrinking), ϕ_0 satisfies

$$\begin{cases} \phi_0(x, y) < 0, & (x, y) \in \Omega_0, \\ \phi_0(x, y) = 0, & (x, y) \in C_0, \\ \phi_0(x, y) > 0, & (x, y) \in \mathbb{R}^2 \setminus \bar{\Omega}_0, \end{cases}$$

and Ω_0 is the region delimited by C_0 .

Typically, the evolution governed by equation (2.4) can be unstable. The gradient of ϕ can become unbounded or zero, which prevents ϕ from being preserved as a signed distance function and leads segmentation failure. To address this issue, one popular method is re-initialization[6], which consists the following two parts.

- (i) Choose a good initial value: A good choice of ϕ_0 is the signed distance function to an initial given curve C_0 surrounding the objects, which is given by

$$\begin{cases} \phi_0(x, y) = +d((x, y), C_0), & (x, y) \in \Omega_0, \\ \phi_0(x, y) = -d((x, y), C_0), & (x, y) \in \mathbb{R}^2 \setminus \bar{\Omega}_0, \end{cases}$$

where $d((x, y), C_0)$ is the Euclidean distance between the point (x, y) and the curve C_0 .

- (ii) Re-initialization: When the gradient of ϕ tends to become irregular, one can restart the evolution with a new initial value ϕ_0 , which is the steady solution of the Eikonal equation

$$(2.5) \quad \begin{cases} \frac{\partial \phi}{\partial t} = \text{sign}(\phi(x, y, \tilde{t}_0))(1 - |\nabla \phi|), & (x, y, t) \in \Omega \times (0, T], \\ \phi(x, y, 0) = \phi(x, y, \tilde{t}_0), & (x, y) \in \Omega, \end{cases}$$

where $\phi(x, y, \tilde{t}_0)$ is the currently updated level set function. The steady solution of (2.5) satisfies $|\nabla \phi| = 1$, which can ensure ϕ satisfies the property of the signed distance function over a period of time.

However, in real implementation, re-initialization faces the some difficulties: (i) The re-initialization process needs to be done on a regular basis. The rule of when and how to use it is unknown. (ii)The equation (2.5) is a nonlinear hyperbolic equation that presents challenges in dealing with discontinuity and nondifferentiability. When the equation is transformed into a time-dependent problem, the CFL condition [14] for finite propagation velocity and time stability may require many time steps for the solution to converge to the entire domain. When considered as a stable boundary value problem, the existence of discontinuity can seriously affect the design of upwind difference schemes and some fast algorithms. Although the emergence of fast sweeping method [43] provides a good solution for this kind of problem, it still faces development difficulties in practical applications.

2.2. Distance regularization term for re-initialization-free. It can be observed that the intention of re-initialization method is to control $|\nabla \phi|$ within a certain range during the evolution process and thus guarantee the stability of the evolution. Another natural idea is to constrain $|\nabla \phi|$ by the regularization term under the framework of the variational level set method, which formulates the segmentation problem as an energy minimization problem and

incorporates prior knowledge [23, 36] or constraints to improve the accuracy and stability [18, 5, 10].

To illustrate our motivation, we briefly recall some representative distance regularization methods. For simplicity, we assume that $x \in \Omega \subset \mathbb{R}^2$ in the following. In [19], Li *et al* proposed DR1 regularization term

$$(2.6) \quad \mathcal{R}_1(\phi) = \int_{\Omega} r_1(|\nabla\phi|)dx,$$

where $r_1(s) = \frac{1}{2}(s-1)^2$. The gradient flow of (2.6) is

$$(2.7) \quad \frac{\partial\phi}{\partial t} = \operatorname{div}(d_1(|\nabla\phi|)\nabla\phi),$$

where $d_1(s) = 1 - 1/s$. The evolution equation (2.7) has an undesirable side effect. When $|\nabla\phi| \rightarrow 0$, the diffusion rate $(1 - \frac{1}{|\nabla\phi|}) \rightarrow -\infty$ (Figure 1). This causes strong backward diffusion, resulting in oscillations of ϕ . To avoid this, Li *et al* proposed the double-well regularization term (DR2)

$$(2.8) \quad \mathcal{R}_2(\phi) = \int_{\Omega} r_2(|\nabla\phi|)dx,$$

where

$$r_2(s) = \begin{cases} (1 - \cos(2\pi s))/(2\pi)^2, & \text{if } s \leq 1, \\ (s-1)^2/2, & \text{if } s > 1. \end{cases}$$

The corresponding gradient flow is

$$(2.9) \quad \frac{\partial\phi}{\partial t} = \operatorname{div}(d_2(|\nabla\phi|)\nabla\phi),$$

where

$$d_2(s) = \begin{cases} \sin(2\pi s)/(2\pi s), & \text{if } s \leq 1, \\ 1 - 1/s, & \text{if } s > 1. \end{cases}$$

Different from the DR1, the DR2 constrains $|\nabla\phi|$ to 0 or 1, and the coefficient of (2.9) approaches 0 when $|\nabla\phi|$ approaches 0 (Figure 1), which modify the oscillation of the DR1 when $|\phi|$ is very small. At the same time, DR2 could cause the desired sign distance function around zero level set because of the design of function r_2 at $|\nabla\phi| > 1/2$.

Despite the success of the re-initialization-free DR method, there are still some issues that need to be addressed. According to the experimental results, the gradient amplitude of the level set function ϕ does not approach a value close enough to 1. Additionally, both regularization term rely on first-order derivatives. The arc length term constrains $|\nabla\phi|$ to approach 0 near the zero level set region, while the distance regularization term enforces $|\nabla\phi|$ to approach 1. Balancing these two terms can be a challenging task. To address these issues, we propose higher order regularization term based on MBE equation. This approach can provide a theoretical and physical foundation for the development of the model.

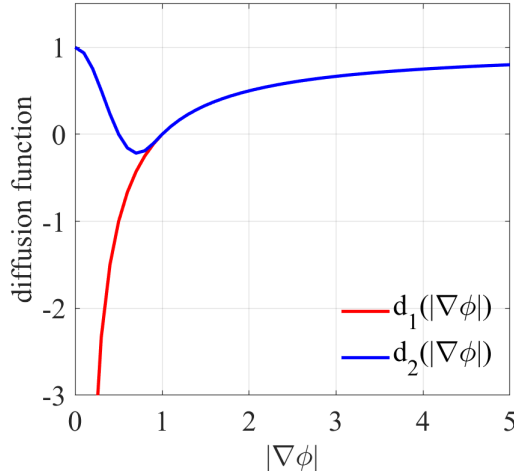


Figure 1. The plots of the diffusion coefficient of the DR1, DR2 of $|\nabla\phi|$.

2.3. Molecular Beam Epitaxy regularization term. The molecular beam epitaxy (MBE) technique is renowned for its precision in growing thin solid films, enabling the formation of monolayer-thin interfaces and atomically flat surfaces [26]. The MBE equation is a fourth-order partial differential equation that ensures the level set function's gradient magnitude approaches 1 while maintaining the desired signed distance function around the zero level set.

Consider the MBE equation with slope selection, which represents the epitaxial growth of thin films, which can be derived from the following functional

$$(2.10) \quad \mathcal{E}_{MBE}(\phi) = \int_{\Omega} \frac{\alpha}{2} |\Delta\phi|^2 + \frac{1}{4} (|\nabla\phi|^2 - 1)^2 dx,$$

where $\phi = \phi(x, t)$ is a scaled height function of a thin film in a co-moving frame,

The MBE model usually has the physical characteristics of unconditional energy stability and unique solution, and the slope can be selected according to the actual research needs. $\mathcal{E}_{MBE}(\phi)$ as the effect free energy, is an example of energy functional of ϕ in the strain gradient theory for structural phase transitions in solids. The second term of $\mathcal{E}_{MBE}(\phi)$ clearly shows the non-equilibrium term of (2.10) forces $|\nabla\phi|$ approach 1.

We compare the MBE regularization term with different regularization terms under the same conditions. Experiments show that the range of the gradient of level set function of MBE regularization tends to be small than that of other regularization terms. See for instance, the MBE regularization term is steadily approaching 1 within a range from 0 to 5, while the range of DR1 becomes from 0 to 16, see Figure 2.

Furthermore, the MBE equation possesses properties that correspond to various image features. For instance, the biharmonic term in the equation contributes to smoothness, reducing noise and irregularities on the thin film surface. This leads to smoother images that are more resistant to noise. Additionally, the non-equilibrium diffusion term treats the thin film surface as a distance function, which preserves its shape and position, similar to preserving the shape and position of image edges. This makes it useful for segmenting objects with

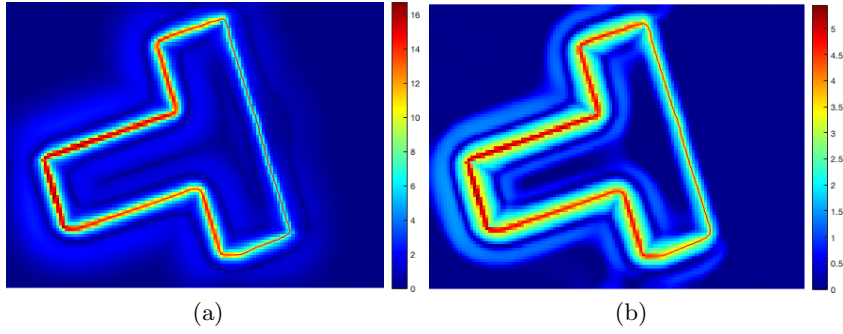


Figure 2. The $|\nabla\phi|$ of segmentation result of different regularization term: (a)DR1 (b)MBE

complex shapes while retaining image information. Finally, the parameters of the equation can be adjusted to achieve the best segmentation effect that meets practical needs.

In summary, the physical principle of the MBE equation is aligned with the objective of re-initializing the level set function. The embedding function (i.e., the film growth height function) is neither too flat nor too steep. Therefore, we apply the MBE equation to the level set method as the regularization term of the level set segmentation model to avoid the need for re-initialization and regulate the smooth of the segmented curve.

3. Main method. In this section, we present a general framework for variational segmentation level set methods integrated with the MBE distance regularization term. Consider the general form of variational level set segmentation model

$$(3.1) \quad \mathcal{E}(\phi) = \mathcal{S}(\phi, I) + \mu\mathcal{R}(\phi) + \nu\mathcal{L}(\phi),$$

where $I : \Omega \rightarrow \mathbb{R}$ is a given vector valued image, $\mathcal{S}(\phi, I)$ is called segmentation term or data fidelity term, $\mathcal{R}(\phi)$ is the regularization term, $\mathcal{L}(\phi)$ is the arc length term and ν, μ are the parameters to adjust the length and smoothness of the curve.

Next, we propose the novel MBE regularization term and present two relevant segmentation models. The regularization term we propose in (3.1) is designed to avoid re-initialization of the segmentation procedure and keep the evolution process accurate and stable. To demonstrate this, we apply the MBE regularization term to the geodesic active contour (GAC) model [3] and the region-scalable fitting (RSF) model [18] and illustrate the superiority of using the MBE regularization term.

3.1. The MBE regularization term. Denote the MBE functional as

$$(3.2) \quad \mathcal{R}_{MBE} = \int_{\Omega} \frac{\alpha}{2} |\Delta\phi|^2 + \frac{1}{4} (|\nabla\phi|^2 - 1)^2 dx.$$

The L^2 gradient flow of (3.2) is

$$(3.3) \quad \begin{cases} \frac{\partial\phi}{\partial t} = -\alpha\Delta^2\phi + \operatorname{div}((|\nabla\phi|^2 - 1)\nabla\phi), & (x, t) \in \Omega \times (0, T], \\ \phi(x, 0) = \phi_0(x), & x \in \Omega, \end{cases}$$

supplemented with suitable boundary conditions, which is the MBE equation with slope selection.

The first term in the right side of equation (3.3) is the equilibrium term, which is the surface diffusion current that describes surface diffusion driven by surface tension. This term, which is of fourth order, represents the equilibrium situation, and α is the surface diffusion constant. The second term (a nonlinear second-order term) in the right side of equation (3.3) is the non-equilibrium diffusion current that depends on the local slope $|\nabla\phi|$. This term is caused by the Ehrlich-Schwoebel instability, which selects the slope of the film surface. The diffusion term of the MBE equation is nonlinear and can describe the nonlinear behaviors of substance diffusion, aggregation, and recrystallization on thin film surfaces. For small slopes, this current is positive, making initially flat interfaces unstable. However, the current vanishes where the slope is 1, which is the preferred slope [26]. Actually, the physical principles of the MBE equation are consistent with the constraint that the level set function is a distance function. Essentially, both require that the level set function (thin film growth height function) ϕ is neither too flat nor too sharp, meaning that the $|\nabla\phi|$ should approach 1 as much as possible.

To illustrate the necessity of fourth-order terms in the MBE regularization term, we analyze the following two cases. On the one hand, when $\alpha = 0$, the diffusion rate is proportional to $(|\nabla\phi|^2 - 1)$. If $|\nabla\phi| > 1$, the diffusion rate is positive and the effect is similar to usual diffusion, which makes the level set function more even and reduces $|\nabla\phi|$. However, if $|\nabla\phi| < 1$, the diffusion term has a reverse effect and may increase the gradient. This can result in an ill-posed equation, where $|\nabla\phi|$ cannot be well-controlled within a stable range. On the other hand, when $\alpha \neq 0$, the term $-\alpha\Delta^2\phi$ acts as a type of viscous term that provides a well-controlled mechanism for diffusion. Specifically, the fourth-order regularization term can penalize changes in second-order curvature, resulting in a segmentation result with continuity and smoothness. This regularization term can reduce noise and discontinuity in the segmentation results, while preserving more details.

Therefore, the MBE equation imposes a stronger smoothness requirement than isotropic and anisotropic diffusion models, thus eliminating the staircase effect. It can also be combined with a L^2 fidelity term to generate piecewise linear solutions [11]. In addition, the MBE equation predicts that mound-like or pyramid structures in the surface profile will tend to have a uniform, constant mound slope [26, 15, 27], which ensuring the smooth of the evolution.

Overall, by incorporating this higher order regularization framework, the need for re-initialization procedures can be eliminated and the evolution will be more accurate and stable. Meanwhile, the MBE equation satisfies the energy dissipation law, which facilitates the acquisition of numerical schemes. The unconditional stability of the energy dissipation maintenance scheme allows for flexibility in model processing.

3.2. Two applications of MBE regularization method.

3.2.1. The MBE-GAC model. The GAC model [3] is a popular image segmentation method that incorporates a geodesic distance term, which is a commonly used data fidelity term.

Let $\delta(\cdot)$ be the Dirac function, $H(\cdot)$ be the Heaviside function [37],

$$(3.4) \quad H(\phi) = \begin{cases} 1, & \text{if } \phi \geq 0, \\ 0, & \text{if } \phi < 0, \end{cases}$$

and $g = \frac{1}{1 + |\nabla G_\sigma * I|^2}$ is the edge detection function. Rewriting GAC model as

$$\mathcal{S}_{GAC}(\phi) = \lambda \int_{\Omega} g\delta(\phi)|\nabla\phi|dx + \gamma \int_{\Omega} gH(-\phi)dx,$$

we propose the MBE-GAC model

$$\mathcal{E}_{MBE-GAC}(\phi) = \mathcal{S}_{GAC}(\phi) + \mu\mathcal{R}_{MBE}(\phi).$$

Denoting $F_{GAC}(\phi) = \lambda\delta(\phi) \operatorname{div}\left(g\frac{\nabla\phi}{|\nabla\phi|}\right) + \gamma g\delta(\phi)$, one derives the corresponding L^2 gradient flow as

$$(3.5) \quad \begin{cases} \frac{\partial\phi}{\partial t} = \mu(-\alpha\Delta^2\phi + \operatorname{div}((|\nabla\phi|^2 - 1)\nabla\phi)) + F_{GAC}(\phi), & (x, t) \in \Omega \times (0, T], \\ \phi(x, 0) = \phi_0(x), & x \in \Omega, \end{cases}$$

supplemented with suitable boundary conditions. The energy functional corresponding to the GAC model can actually be regarded as the arc length with weights, so the MBE-GAC model contains only data fidelity term and regularization term.

The original GAC model does not depend on the parameters of the curve, but sensitive to the selection of the initial position, and only works for convex boundaries of object. Coupling MBE regularization term, the new MBE-GAC model does not rely on the selection of the initial position and have good segmentation performance when the edge of the segmented object containing sag.

3.2.2. The MBE-RSF model. The RSF model has achieved good performance in handling the image of heterogeneous regions. It is a two-phase segmentation method that uses two fitting functions, denoted by f_1 and f_2 , to approximate the image intensity on both sides of the object boundary. The data fidelity term is then formulated based on the difference between the image intensity and the fitting functions inside the boundary of object, forcing the evolution towards the object boundary.

Let C is the closed curve separating the region Ω , $\Omega_1 = \text{inside}(C)$, $\Omega_2 = \text{outside}(C)$, the locally fitting function can be represented as

$$\mathcal{S}_x(C, f_1, f_2) = \sum_{i=1}^2 \lambda_i \int_{\Omega_i} K_\sigma(x-y)|I(y) - f_i(x)|^2 dx,$$

where λ_1, λ_2 are positive constants and $K_\sigma(u) = \frac{1}{(2\pi)^{n/2}\sigma^2} \exp(-|u|^2/2\sigma^2)$ is the kernel function. Integrating $\mathcal{S}_x(C, f_1, f_2)$ over the image domain Ω and by [18], one derives RSF

fidelity term

$$\mathcal{S}_{RSF}(\phi, f_1, f_2) = \sum_{i=1}^2 \lambda_i \int_{\Omega} \int_{\Omega} K_{\sigma}(x-y) |I(y) - f_i(x)|^2 M_i(\phi(y)) dy dx,$$

where $M_1(\phi) = H(\phi)$ and $M_2(\phi) = 1 - H(\phi)$.

Different from MBE-GAC model, when using the RSF model, it is necessary to add the arc length term to eliminate the effect of noise. Usually, $\mathcal{L}(\phi)$ measures the arc length of the zero level curve which is defined by

$$(3.6) \quad \mathcal{L}(\phi) = \int_{\Omega} |\nabla H(\phi)| dx = \int_{\Omega} \delta(\phi) |\nabla \phi| dx.$$

The arc length term penalizes the curvature of the curve, resulting in a smoother and more natural curve shape while suppressing local details and noise.

Overall, we derive the MBE-RSF model as

$$(3.7) \quad \mathcal{E}_{MBE-RSF}(\phi, f_1, f_2) = \mathcal{S}_{RSF} + \mu \mathcal{R}_{MBE} + \nu \mathcal{L}.$$

Consequently, set

$$F_{RSF}(\phi) = -\delta(\phi)(\lambda_1 e_1 - \lambda_2 e_2) + \nu \delta(\phi) \operatorname{div}\left(\frac{\nabla \phi}{|\nabla \phi|}\right).$$

The corresponding L^2 gradient flow of (3.7) is

$$(3.8) \quad \begin{cases} \frac{\partial \phi}{\partial t} = \mu(-\alpha \Delta^2 \phi + \operatorname{div}((|\nabla \phi|^2 - 1)\nabla \phi)) + F_{RSF}(\phi), & (x, t) \in \Omega \times (0, T], \\ \phi(x, 0) = \phi_0(x), & x \in \Omega, \end{cases}$$

supplemented with suitable boundary conditions, where

$$e_i = \int_{\Omega} K_{\sigma}(y-x) |I(x) - f_i(y)|^2 dy, \quad i = 1, 2,$$

and

$$f_i(x) = \frac{K_{\sigma}(x) * [M_i(\phi(x))I(x)]}{K_{\sigma} * M_i(\phi(x))}, \quad i = 1, 2.$$

The original RSF model used the DR1 regularization term. Replacing DR1 regularization term with MBE regularization term, one can obtain better controls on the range of variation and obtain more accurate results.

4. Numerical algorithms. The numerical implementation is carried out by solving the gradient descent flow of the model (3.1). In general, for high-order nonlinear problems, the convergence condition of explicit scheme is harsh, resulting in low computational efficiency. The implicit scheme is stable, but the solution process is challenging as it involves solving a nonlinear steady equation at each time step. Usually, semi-implicit and semi-explicit finite difference scheme is widely used in such problems, see for instance [16, 9].

Let $h = 1$ be the space grid size, τ be the times step, and denote

$$x_i = ih, i = 1, 2, \dots, M, \quad y_j = jh, j = 1, 2, \dots, N, \quad t_n = n\tau, n = 0, 1, \dots$$

where $M \times N$ is the size of the image support. For simplicity, we denote the segmentation term and arc length term in model (3.5) and (3.8) as $T_{seg}(\phi)$. We first generalize the semi-implicit and semi-explicit discretization given in [15] to the proposed MBE-based model as

$$(4.1) \quad \begin{aligned} & \frac{\phi_{i,j}^{n+1} - \phi_{i,j}^n}{\tau} + \mu \left(\frac{3}{4} \alpha \Delta^2 \phi_{i,j}^{n+1} + \Delta \phi_{i,j}^{n+1} \right) \\ & = \mu \left(-\frac{\alpha}{4} \Delta^2 \phi_{i,j}^n + \operatorname{div}(|\nabla \phi_{i,j}^n|^2 \nabla \phi_{i,j}^n) \right) + T_{seg}(\phi_{i,j}^n), \end{aligned}$$

where $\phi_{i,j}^n = \phi(x_i, y_j, \tau_n)$ denotes the discretization of ϕ . Experiments have revealed the accuracy of the scheme (4.1). However, due to the high order of the linear term and the complexity of the nonlinear terms, the time step τ should be small enough to ensure the stability, which limits the applications of scheme (4.1) in real implementation by its low efficiency.

The scalar auxiliary variable (SAV) method [32] is unconditionally energy stable for solving gradient flows with no restrictions on the specific form of the nonlinear terms. By introducing an auxiliary variable that do not depend on spatial variables, the SAV scheme for the proposed MBE segmentation model only involves solving two linear equations with constant coefficients and the accuracy does not depend on the choice of the time step τ . Besides, the resulting linear equations of our model can be easily solved by the fast Fourier transform (FFT) algorithm [13]. Thus, in this section, we derive the scalar auxiliary variable (SAV) for the proposed segmentation model. Compared with the traditional semi-implicit and semi-explicit scheme (4.1), the SAV scheme for the MBE segmentation model is easier to implement and can significantly improve the computational efficiency.

4.1. Scalar auxiliary variable (SAV) scheme. As we know, the SAV is a new technique to construct time discretization schemes for a class of gradient flows driven by a bounded free energy functional $\mathcal{E}(\phi)$ from below. Obviously, in both MBE-GAC model and MBE-RSF model, there exists a positive constants C_0 such that $\mathcal{E}_1(\phi) \geq C_0 > 0$. To illustrate the idea, we rewrite the variational level set model (3.1) in the general form,

$$\mathcal{E}(\phi) = \frac{1}{2}(\phi, \mathcal{L}\phi) + \mathcal{E}_1(\phi),$$

where $\mathcal{L} = \mu\alpha\Delta^2$ is a symmetric non-negative linear operator independent of ϕ , and $\mathcal{E}_1(\phi)$ contains other lower order operators in (3.1).

Introduce a scalar auxiliary variable $r = \sqrt{\mathcal{E}_1(\phi)}$ and rewrite the L^2 gradient flow (3.5) or

(3.8) as

$$(4.2a) \quad \frac{\partial \phi}{\partial t} = -\omega,$$

$$(4.2b) \quad \omega = \mathcal{L}\phi + \frac{r}{\sqrt{\mathcal{E}_1(\phi)}}U(\phi),$$

$$(4.2c) \quad \frac{dr}{dt} = \frac{1}{2\sqrt{\mathcal{E}_1(\phi)}} \int_{\Omega} U \frac{\partial \phi}{\partial t} dx,$$

According to the standard procedure given in [32, 39], taking the time step τ , we derive the following first-order SAV scheme

$$(4.3a) \quad \frac{\phi^{n+1} - \phi^n}{\tau} = -\omega^{n+1},$$

$$(4.3b) \quad \omega^{n+1} = \mathcal{L}\phi^{n+1} + \frac{r^{n+1}}{\sqrt{\mathcal{E}_1(\phi^n)}}U(\phi^n),$$

$$(4.3c) \quad \frac{r^{n+1} - r^n}{\tau} = \frac{1}{2\sqrt{\mathcal{E}_1(\phi^n)}} \int_{\Omega} U(\phi^n) \frac{\phi^{n+1} - \phi^n}{\tau} dx.$$

A major advantage of SAV scheme is that it is easy to implement. In fact, substituting (4.3b) and (4.3c) into (4.3a) and put the terms consisting ϕ^{n+1} on the left hand side, then

$$(4.4) \quad (I + \tau\mathcal{L})\phi^{n+1} + \frac{\tau}{2}b^n(b^n, \phi^{n+1}) = c^n.$$

where $b^n = U(\phi^n)/\sqrt{\mathcal{E}_1(\phi^n)}$ and $c^n = \phi^n - \tau r^n b^n + \frac{\tau}{2}(b^n, \phi^n)b^n$ are know quantities.

To obtain ϕ^{n+1} , denote $(I + \tau\mathcal{L})$ by A . Multiplying (4.4) with A^{-1} and taking the inner product with b^n , one finds

$$(4.5) \quad (b^n, \phi^{n+1}) = \frac{(b^n, A^{-1}c^n)}{1 + \tau/2(b^n, A^{-1}b^n)} := d^n.$$

Combining with (4.4) and (4.5) gives

$$(4.6) \quad \phi^{n+1} = A^{-1} \left(c^n - \frac{\tau}{2}b^n d^n \right).$$

We sum up the above SAV scheme as [Algorithm 4.1](#)

Algorithm 4.1 SAV algorithm of MBE-RSF model

Input: $\phi_0, \tau, \text{numIter}$, model parameters

For $n = 1$ to numIter

Update ϕ^{n+1} according the initial function ϕ_0

Calculate $b^n = U(\phi^n)/\sqrt{\mathcal{E}_1(\phi^n)}$ and c^n (the righthand side of (4.4))

Let $A = I + \tau\mathcal{L}$ and calculate (b^n, ϕ^{n+1}) from (4.5)

Calculate ϕ^{n+1} from (4.6)

Multiplying the equations (4.3) by ω^{n+1} , $(\phi^{n+1} - \phi^n)/\tau$, $2r^{n+1}$, integrating the first two equations, and adding them together, we obtain the following stability result.

Theorem 4.1. *The SAV scheme (4.3) is first-order unconditionally energy stable in the sense that:*

$$\begin{aligned} & \frac{1}{\tau} \left(\tilde{\mathcal{E}}(\phi^{n+1}, r^{n+1}) - \tilde{\mathcal{E}}(\phi^n, r^n) \right) \\ & + \frac{1}{\tau} \left(\frac{1}{2} (\phi^{n+1} - \phi^n, \mathcal{L}(\phi^{n+1} - \phi^n)) + (r^{n+1} - r^n)^2 \right) = -(\omega^{n+1}, \omega^{n+1}), \end{aligned}$$

where $\tilde{\mathcal{E}}(\eta, r) = \frac{1}{2} (\eta, \mathcal{L}\eta) + r^2$ is the modified energy.

4.2. The discretization of space. We employ the $n+1$ level data only some of the linear terms, and the others we employ the n level data, which confirms we could use discrete Fourier transform to solve the ϕ^{n+1} . Define the discrete backward and forward differential operators with periodic boundary condition as follows:

$$\begin{aligned} \partial_1^- \phi_{i,j} &= \begin{cases} \phi_{i,j} - \phi_{i-1,j}, & 1 < i \leq M, \\ \phi_{1,j} - \phi_{M,j}, & i = 1, \end{cases} \\ \partial_1^+ \phi_{i,j} &= \begin{cases} \phi_{i+1,j} - \phi_{i,j}, & 1 \leq i < M, \\ \phi_{1,j} - \phi_{M,j}, & i = M, \end{cases} \\ \partial_2^- \phi_{i,j} &= \begin{cases} \phi_{i,j} - \phi_{i,j-1}, & 1 < j \leq N, \\ \phi_{i,1} - \phi_{i,N}, & j = 1, \end{cases} \\ \partial_2^+ \phi_{i,j} &= \begin{cases} \phi_{i,j+1} - \phi_{i,j}, & 1 \leq j < N, \\ \phi_{i,1} - \phi_{i,N}, & j = N, \end{cases} \end{aligned}$$

and the central difference operators, the gradient, divergence, Laplace, and biharmonic operators are defined accordingly as

$$\begin{aligned} \partial_1^c \phi_{i,j} &= (\partial_1^- \phi_{i,j} + \partial_1^+ \phi_{i,j})/2, \\ \partial_2^c \phi_{i,j} &= (\partial_2^- \phi_{i,j} + \partial_2^+ \phi_{i,j})/2, \\ \nabla^c \phi_{i,j} &= \langle \partial_1^c \phi_{i,j}, \partial_2^c \phi_{i,j} \rangle, \\ \operatorname{div}^c(\langle \phi_{i,j}, \psi_{i,j} \rangle) &= \partial_1^c \phi_{i,j} + \partial_2^c \psi_{i,j}, \\ \Delta^c \phi_{i,j} &= \partial_1^+ \partial_1^- \phi_{i,j} + \partial_2^+ \partial_2^- \phi_{i,j}, \\ \Delta^{2c} \phi_{i,j} &= \Delta^c \Delta^c \phi_{i,j}. \end{aligned}$$

As the low computational efficiency of finite difference schemes for fourth-order equations, we apply the discrete Fourier transform \mathcal{F} to both sides [13],

$$(4.7) \quad \begin{aligned} \mathcal{F} \partial_1^\pm \phi_{i,j} &= \pm (e^{\pm \sqrt{-1} z_i^1} - 1) \mathcal{F} \phi_{i,j}, \\ \mathcal{F} \partial_2^\pm \phi_{i,j} &= \pm (e^{\pm \sqrt{-1} z_j^2} - 1) \mathcal{F} \phi_{i,j}, \end{aligned}$$

where $z_i^1 = 2\pi(i-1)/M, i = 1, 2, \dots, M, z_j^2 = 2\pi(j-1)/N, j = 1, 2, \dots, N$.

Therefore, once $\mathcal{F} \phi_{i,j}^{n+1}$ is calculated, we can obtain $\phi_{i,j}^{n+1}$ by the discrete inverse Fourier transform (IFFT). Because of the utilize of the FFT, it is efficient to solve the designed numerical scheme.

In addition, the Dirac function $\delta(\phi)$ is approximated by the following forms,

$$(4.8) \quad \delta_{1,\epsilon}(p) = \begin{cases} 0, & p \in \mathbb{R}, \quad |p| > \epsilon, \\ \frac{1}{2\epsilon} \left(1 + \cos\left(\frac{\pi p}{\epsilon}\right)\right), & |p| \leq \epsilon, \end{cases}$$

and

$$(4.9) \quad \delta_{2,\epsilon}(p) = \frac{1}{\pi} \cdot \frac{p}{p^2 + \epsilon^2}, \quad p \in \mathbb{R}.$$

The support of Equation (4.8) is limited, which can cause the level set to become trapped in local minima during evolution. On the other hand, Equation (4.9) acts on all curves, generating new curves and leading to improved global minimum results.

5. Experimental results. In this section, we compare the experimental results of the MBE-GAC and MBE-RSF models for image segmentation. Our findings show that the MBE-GAC model performs well in segmenting images with clear edges, while the MBE-RSF model is more effective for images with fuzzy edges. Moreover, we present the segmentation results obtained using the MBE-RSF model. Comparative experiments indicate that the MBE regularization term is more robust to noise compared to other regularization terms, and eliminates the need for level set re-initialization. Furthermore, the MBE-RSF model is capable of handling a wide range of composite and real images, including medical images and those with complex boundaries and intensity inhomogeneity distributions. These results demonstrate the effectiveness and versatility of the MBE-based models for various image segmentation tasks.

5.1. Independence of initial curve. To verify the independence of the MBE regularization term on the initial curve, we perform an experiment using two composite images with different initial curves. The first image, depicted in Figure 3, is a uniform intensity image. We apply the MBE-GAC model and classical regularization terms with the same parameters to the image. The experimental results show that the MBE regularization term performs similarly to the classical regularization term, but with a smaller range of variation in $|\nabla\phi|$. Moreover, the segmentation results are accurate for different initial curves and can effectively identify the target boundary.

The second image, shown in Figure 4, has heterogeneous regions. We apply the MBE-RSF model to the image and compare its segmentation performance with DR1 regularization term. The experimental results demonstrated that the segmentation curves generated by the MBE-GAC and MBE-RSF models are smoother than those produced by DR1 regularization term. For instance, the boundary curve of the quadrilateral in Figure 4 is smoother than that in Figure 4. Overall, our findings indicate that the MBE regularization term is effective in producing smooth and accurate segmentation results that are independent of the initial curve.

5.2. Property of smooth control. In Figure 7, we use the MBE-RSF model to separate the ring and the background, and the initial curve and its level set function are shown in Figure 5.

In the variational level set method, the coefficient ν of the arc length term controls the degree of smoothing, with larger values leading to higher curve smoothness and smoother shapes. By adjusting the value of ν , the curve shape and smoothness can be flexibly controlled.

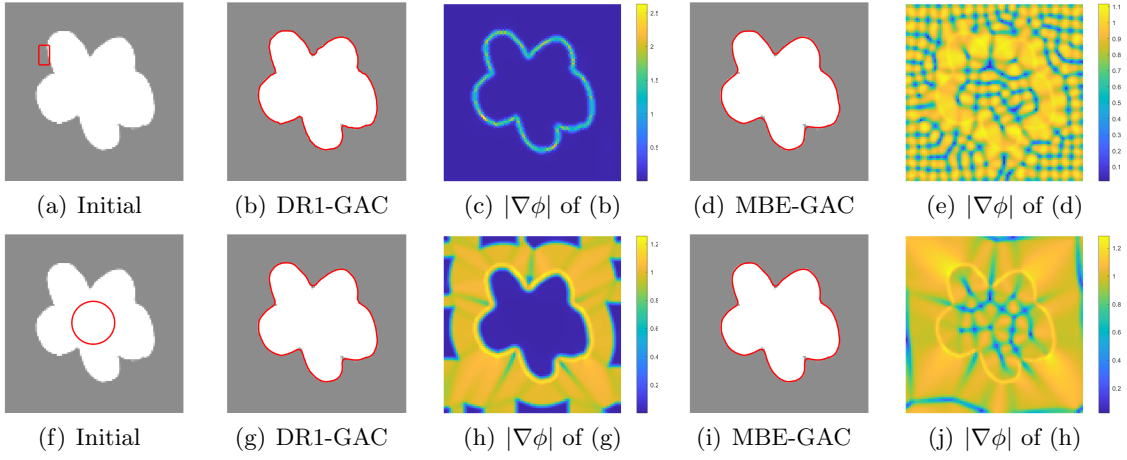


Figure 3. Segmentation results of the DR1-GAC and MBE-GAC with same initial level set functions. Upper row: binary function as the initial level set function; lower row: signed distance function as the initial level set function.

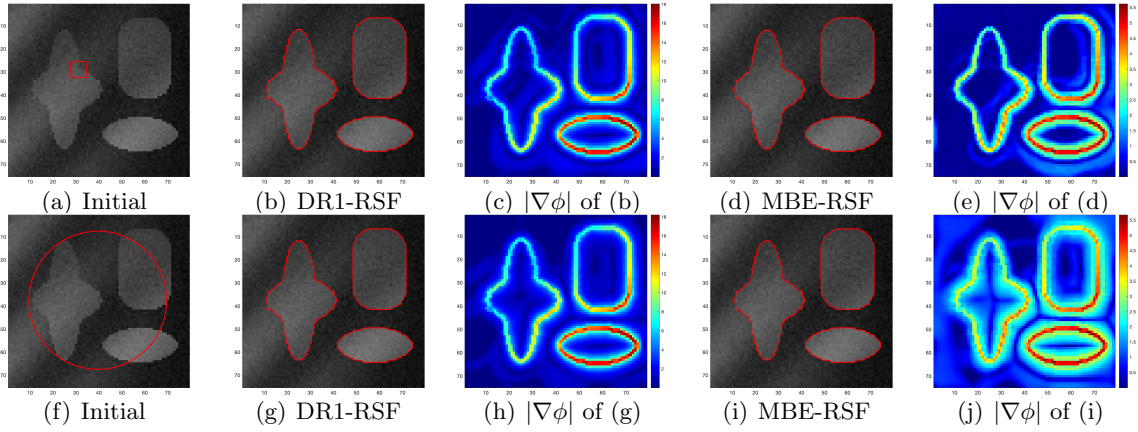


Figure 4. Segmentation results of DR1-RSF model and MBE-RSF model with same initial level set functions. Upper row: binary function as the initial level set function; lower row: signed distance function as the initial level set function.

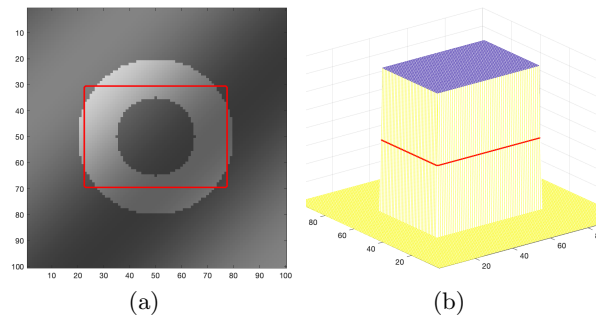


Figure 5. The initial curve and level set function.

We test the MBE regularization term on a boundary-blurred image shown in Figure 6 and set $\lambda_1 = 0.33$, $\lambda_2 = 0.67$, $\epsilon = 1$, $\sigma = 3$, $\tau = 0.01$, $iter = 2000$. Our experimental results show that even when $\nu = 0$, the biharmonic term can still ensure the smoothness of the segmentation curve and requires fewer iterations. However, lowering the bi-harmonic term parameter μ can lead to some erroneous segmentation results, as seen in images Figure 6(d) and Figure 6(e). This suggests that the fourth-order term in the MBE equation has a greater control over the segmentation results than the biharmonic term when μ is low.

Based on these findings, we plan to further explore the smooth control characteristics of the MBE regularization term. Specifically, we will investigate how the different terms in the MBE equation affect the smoothness and accuracy of the segmentation results under different parameter settings. This will enable us to better understand the behavior of the MBE regularization term and improve its performance in various segmentation tasks.

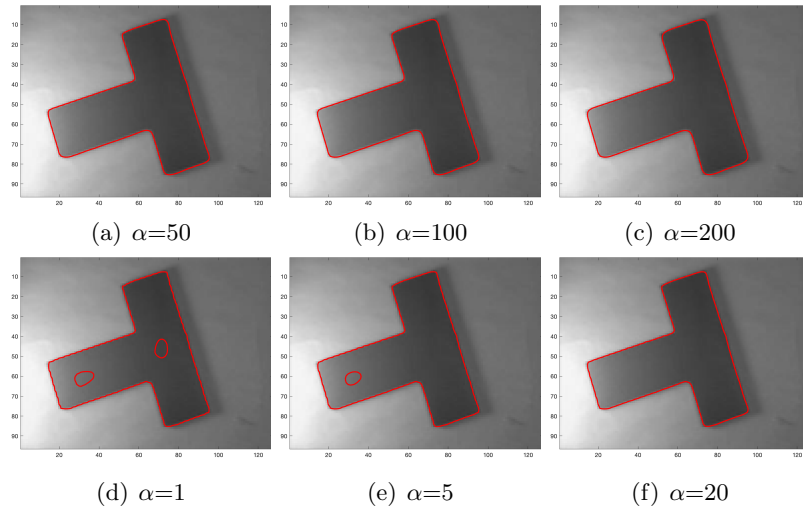


Figure 6. Segmentation results of the MBE-RSF model. Upper row: results without arc length term; lower row: results with arc length term when $\nu = 10$

Table 1
Parameters of Figure 6.

| | λ_1 | λ_2 | μ | α | ν | τ | iter |
|------|-------------|-------------|-------|----------|-------|--------|-------|
| 6(a) | 1 | 2 | 1 | 50 | 0 | 0.01 | 3000 |
| 6(b) | 1 | 2 | 1 | 100 | 0 | 0.01 | 3000 |
| 6(c) | 1 | 2 | 1 | 200 | 0 | 0.01 | 3000 |
| 6(d) | 1 | 3 | 1 | 1 | 10 | 0.01 | 10000 |
| 6(e) | 1 | 3 | 1 | 5 | 10 | 0.01 | 10000 |
| 6(f) | 1 | 3 | 1 | 20 | 10 | 0.01 | 10000 |

We set $\mu = 1$, $\tau = 0.01$, and find that increasing the coefficient of the bi-harmonic term leads to smoother curves. For example, in Figure 7(b), Figure 7(c), and Figure 7(e),

all parameters except α are kept the same, and the segmentation result of Figure 7(e) is smoother, indicating that the bi-harmonic term can effectively control the smoothness of the curve.

We also set $\alpha = 1, \nu = 0, 10, 500$ for the results shown in Figure 7(a), Figure 7(b), and Figure 7(f), respectively, while keeping other parameters the same. We find that even for $\nu = 500$ in Figure 7(f), the local smoothness of the curves remained the same. This is because the arc-length term used as a regularization term only controls the macroscopic length of the curve, without being able to improve its smoothness locally.

Our experiments with images featuring inhomogeneous intensity showed that, when using the same initial curve lines, the segmentation curve obtained with the MBE regularization model was smoother than that obtained with the DR2-RSF model, with fewer thorns in the curve lines. This suggests that the MBE-based model, which incorporates a bi-harmonic regularization term, is better suited to promote the smoothness and continuity of the curve in the presence of intensity variations.

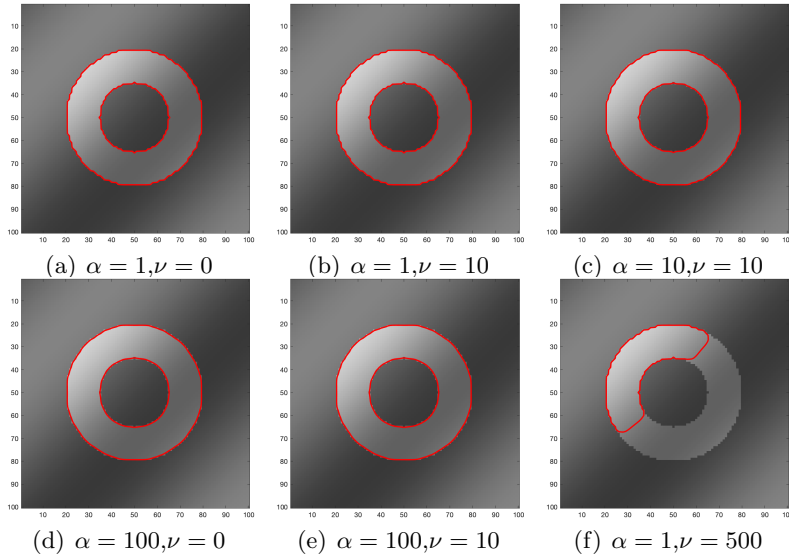


Figure 7. Segmentation results of MBE-RSF model.

Table 2

Parameters of Figure 7. ($\lambda_1 = 0.33, \lambda_2 = 0.67, \epsilon = 1, \sigma = 3, \tau = 0.01$)

| | μ | α | ν | τ | iter |
|-------------|-------|----------|-------|--------|------|
| Figure 7(a) | 1 | 1 | 0 | 0.01 | 2000 |
| Figure 7(b) | 1 | 1 | 10 | 0.01 | 2000 |
| Figure 7(c) | 1 | 10 | 10 | 0.01 | 2000 |
| Figure 7(d) | 1 | 100 | 0 | 0.01 | 2000 |
| Figure 7(e) | 1 | 100 | 10 | 0.01 | 2000 |
| Figure 7(f) | 1 | 1 | 500 | 0.01 | 2000 |

In summary, the MBE regularization term can effectively control the smoothness of the

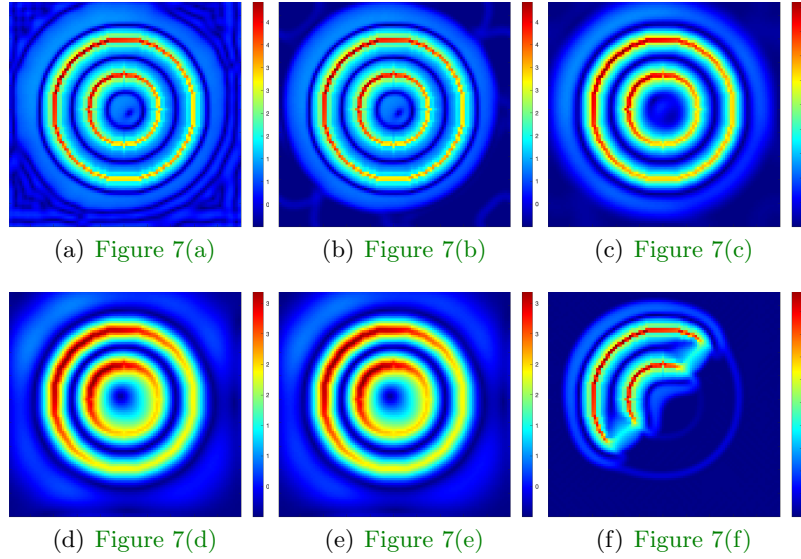


Figure 8. The map of $|\nabla\phi|$ corresponding to Figure 7.

contour by adjusting the biharmonic coefficient α , while the arc-length term only controls the macroscopic length of the curve with little influence on local smoothness. Based on these findings, we plan to further explore the application of the MBE-RSF model in noise image segmentation.

5.3. Property of anti-noise. Image noise is a common problem that can negatively impact the performance of image segmentation models. In order to evaluate the the robustness of the model with respect to noises, we contaminate the original images with Gaussian noise. We apply MBE and DR2 regularization methods to the RSF model and evaluate their segmentation performance on a same noisy image. Results can be compared to determine which regularization method performs better for the specific noise image segmentation problem at hand.

The images to be segmented are shown in Figure 10 and Figure 12, with noise levels of 10 and 15. The initial level and function selection are the same as in Figure 5. In noisy situations, segmentation of non-uniform intensity images is more difficult than that of uniform intensity images. Both models require two fitting function f_1 and f_2 to approximate the image intensities, and some of the noisy speckle would be enlarged during the fitting procedure due to the influence of noise and inhomogeneous background, as shown in Figure 9. The above analysis shows that noise has a great influence on the segmentation results of RSF fitting model, so it is necessary to add a suitable regular term.

The effectiveness of DR2 regularization term in combating noise can be seen in the segmentation results of DR2-RSF and MBE-RSF when the noise level is set to 10, as shown in Figure 10. We set $\lambda_1 = 0.33$, $\lambda_2 = 0.67$ and $\sigma = 5$, the other parameters are shown in Table 3. It is found that the DR2 regularization term is ineffective in combating noise for the segmentation results of the DR2-RSF model always contain spots. The MBE-RSF model can perfectly segment the banded ring, thanks to its ability to control local smoothness and

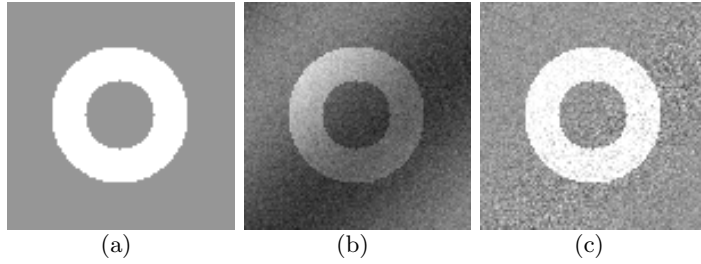


Figure 9. (a)Original homogeneous image; (b)Noisy inhomogeneous image ($std = 10$); (c)Ideally fitted image.

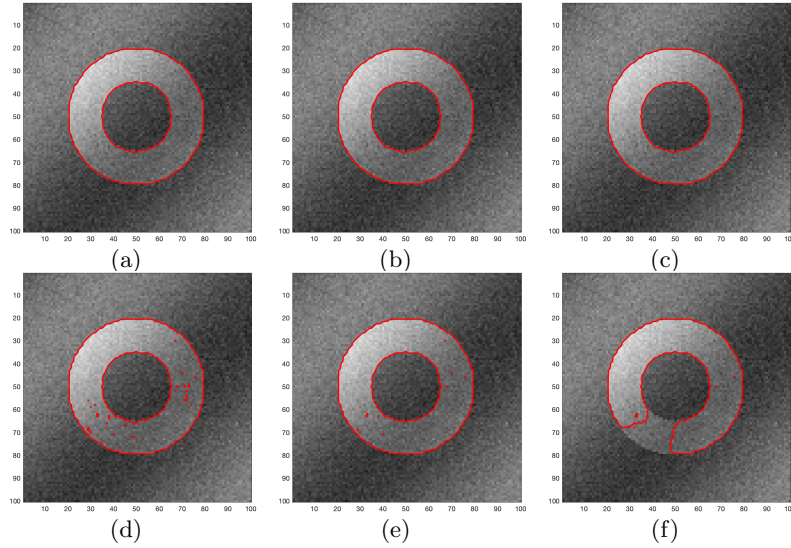


Figure 10. Segmentation results of MBE-RSF model (a)-(c) and DR2-RSF model (d)-(f) for the noisy image ($std = 10$).

anti-noise of the curve using the MBE regularization term. Moreover, the segmentation results of MBE-RSF are robust to different parameter selection conditions, as demonstrated in Figures 10(a) to 10(c). Even when the arc length parameter $\nu = 0$, the model can achieve good segmentation results, further highlighting the advantages of the MBE regularization term.

The segmentation results of the DR2-RSF and MBE-RSF models with a noise level of 15 and parameters set to $\lambda_1 = 0.4$, $\lambda_2 = 0.6$, and $\sigma = 6$ are shown in Figure 12, with the other parameters selected as listed in Table 4. Similar to the case with a noise level of 10, the DR2-RSF model fails to produce smooth segmentation results. As the noise level increases, more artifacts appear at the segmentation boundaries in the DR2-RSF model, indicating that noise has a greater negative impact on its segmentation performance. In contrast, in the absence of arc length constraint, the MBE-RSF model adjusts the coefficients between μ and α to smoothly separate the ring region from the background.

Furthermore, both methods require more iterations to achieve a stable state due to the increased noise level. The experimental results in Figure 12 further highlight the advantages

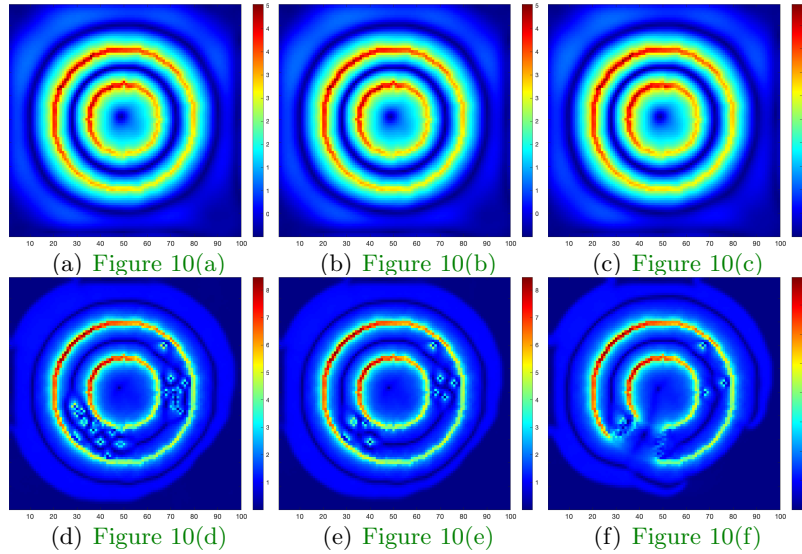


Figure 11. The map of $|\nabla\phi|$ corresponding to Figure 10.

Table 3

Parameters of Figure 10. ($\lambda_1 = 0.33$, $\lambda_2 = 0.67$, $\epsilon = 1$, $\sigma = 5$)

| std.n = 10 | μ | α | ν | τ | iter |
|--------------|-------|----------|-------|--------|------|
| Figure 10(a) | 1 | 15 | 10 | 0.01 | 4000 |
| Figure 10(b) | 1 | 15 | 20 | 0.01 | 4000 |
| Figure 10(c) | 1 | 20 | 0 | 0.01 | 4000 |
| Figure 10(d) | 6.6 | - | 20 | 0.015 | 2000 |
| Figure 10(e) | 6.6 | - | 100 | 0.015 | 2000 |
| Figure 10(f) | 8 | - | 150 | 0.013 | 4000 |

of the MBE regularization method in combating noise.

5.4. MBE-RSF model for real image segmentation. Real images often contain complex structures, various backgrounds, and different lighting conditions, which pose significant challenges to image segmentation. Numerical experiments on real images can also be time-consuming. Therefore, in this section, we use both the semi-implicit semi-explicit finite-difference method (FDM) and the SAV scheme to discretize the images. Our experimental results demonstrate that the MBE-RSF model produces highly accurate segmentation results, even on complex real-world images.

Compared to the DR1/DR2 regularization terms, the MBE-RSF model has shown promising results in natural and medical image segmentation. In natural image segmentation, as shown in Figure 14 and Figure 15, the MBE-RSF model effectively segments objects in complex scenes with varying backgrounds and lighting conditions. The model has also demonstrated its ability to segment objects in challenging scenarios with occlusions and overlapping objects.

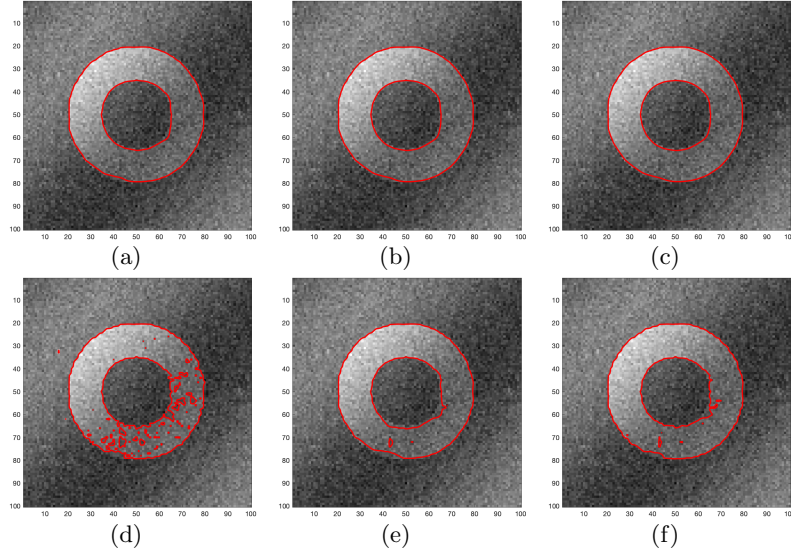


Figure 12. Segmentation results of MBE-RSF model (a)-(c) and DR2-RSF model (d)-(f) for the noisy image ($std = 15$).

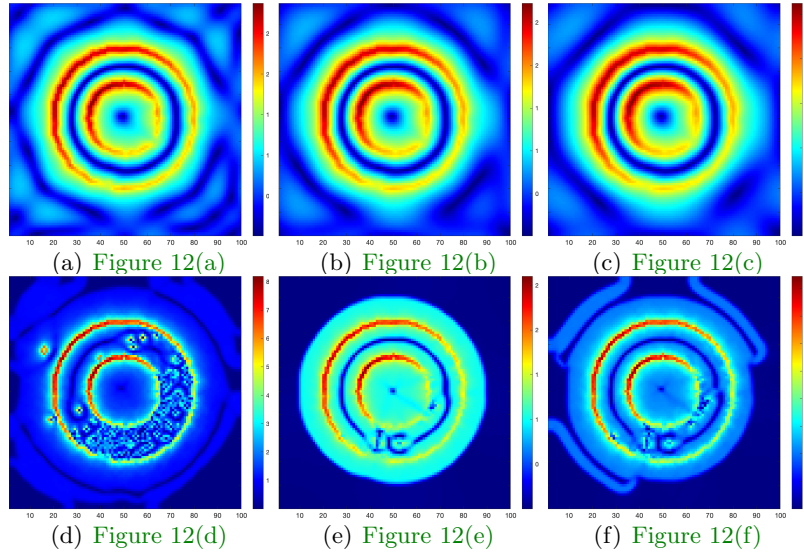


Figure 13. The map of $|\nabla\phi|$ corresponding to Figure 12.

We have also applied the MBE-RSF model to medical image segmentation and compared it with the DR1/DR2-RSF models. To ensure the fairness of the comparison, both models are fine-tuned to achieve optimal segmentation results. Our experimental results show that the MBE-RSF model outperforms the DR1/DR2-RSF models in segmenting low-dose CT images, X-ray images, microscopic cell images, and MRI images.

Figure 16 shows the segmentation results of low-dose lung CT images. Due to the poor

Table 4

Parameters of *Figure 12*. ($\lambda_1 = 0.4$, $\lambda_2 = 0.6$, $\epsilon = 1$, $\sigma = 6$)

| std_n = 15 | μ | δ | ν | τ | iter |
|--------------|-------|----------|-------|--------|-------|
| Figure 12(a) | 10 | 10 | 0 | 0.001 | 20000 |
| Figure 12(b) | 10 | 20 | 0 | 0.001 | 20000 |
| Figure 12(c) | 10 | 30 | 0 | 0.001 | 20000 |
| Figure 12(d) | 7 | - | 1 | 0.012 | 8000 |
| Figure 12(e) | 200 | - | 1 | 0.0005 | 30000 |
| Figure 12(f) | 50 | - | 100 | 0.002 | 10000 |

imaging quality of the image, there are a lot of artifacts and noise in the image, which will increase the difficulty of segmentation. Neither DR1 nor DR2 model can represent the smooth curve of lung, which indicates that DR1 and DR2 regularization terms cannot overcome the influence of artifacts and noise. Due to the function of MBE regularization term, the RSF-MBE model can obtain smooth segmentation curve and successfully separate the alveoli. Consistent with the conclusions of the previous section, this experiment demonstrates the advantage of MBE regularization terms in controlling the smoothness of curves and overcoming the influence of noise. Due to the function of MBE regularization term, the model can control the smoothness of curves without losing small targets.

Figure 17 and Figure 18 show the results of microcellular images and brain MRI images, respectively. Both the proposed model and the comparison model can achieve excellent segmentation results, which verifies the effectiveness of the model. Meanwhile, for microscopic images with blurred edges and brain MRI with rugged edges, the MBE regularization term can achieve fine segmentation while controlling the local smoothness of the curve.

Figure 19 compares the segmentation results of the X-ray images of the hand joints of the three models. The segmentation curve obtained by the MBE-RSF model is more suitable for the edges in the image, and the model can distinguish the joints with weak contrast in the image. This shows that the model proposed in this paper can also obtain more precise segmentation results for images with lower contrast.

6. Conclusions. We propose a regularized level set high order variational method for image segmentation problems integrated with the molecular beam epitaxial film manufacturing, which avoids the re-initialization and enhances the stability of the evolution. Two segmentation models, MBE-GAC and MBE-RSF, are introduced, demonstrating the flexibility of the MBE regularization term. We design the SAV scheme coupled with FFT for the proposed MBE segmentation models, which significantly improves the model’s efficiency. Numerical experiments show that our approach can effectively control the local smoothness of the segmentation curve, is robust against noise and is independent of the initial curve. In addition, The model can handle fuzzy edges, intensity inhomogeneity, and small and complex objects with good segmentation results. Overall, the MBE regularization method shows superiority and potential in image segmentation from both accuracy and efficiency.

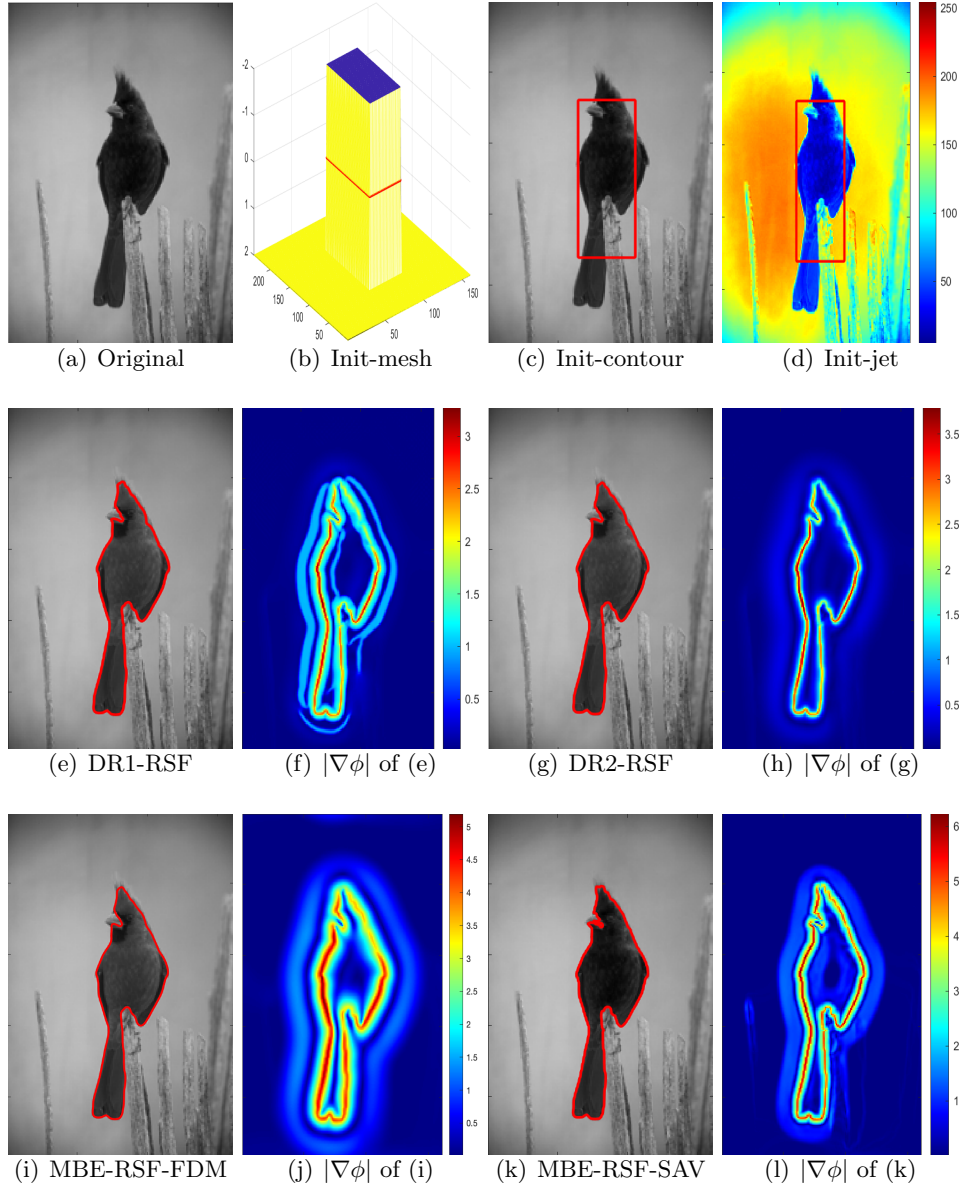


Figure 14. Segmentation results of DR1-RSF model, DR2-RSF model and MBE-RSF model.

Acknowledgments. This work is partially supported by the National Natural Science Foundation of China (12171123, U21B2075, 11971131, 12271130, 11871133), the Natural Science Foundation of Heilongjiang Province (ZD2022A001), the Fundamental Research Funds for the Central Universities (HIT.NSRIF202202, 2022FRFK060020, HIT.NSRIF. 2020081, 2022FRFK060014).

REFERENCES

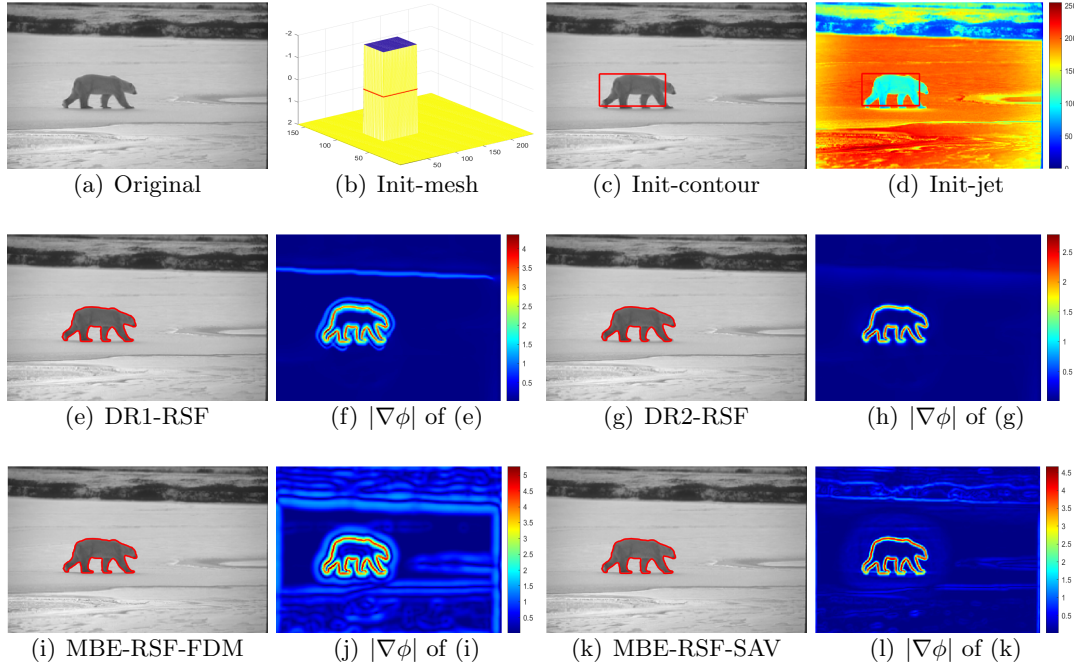


Figure 15. Segmentation results of DR1-RSF model, DR2-RSF model and MBE-RSF model.

- [1] G. AUBERT, P. KORNPBST, AND G. AUBERT, *Mathematical problems in image processing: partial differential equations and the calculus of variations*, vol. 147, Springer, 2006.
- [2] J. CARDELINO, V. CASELLES, M. BERTALMIO, AND G. RANDALL, *A contrario selection of optimal partitions for image segmentation*, SIAM Journal on Imaging Sciences, 6 (2013), pp. 1274–1317.
- [3] V. CASELLES, R. KIMMEL, AND G. SAPIRO, *Geodesic active contours*, International journal of computer vision, 22 (1997), pp. 61–79.
- [4] T. F. CHAN AND L. A. VESE, *Active contours without edges*, IEEE Transactions on image processing, 10 (2001), pp. 266–277.
- [5] Y. CHEN, H. D. TAGARE, S. THIRUVENKADAM, F. HUANG, D. WILSON, K. S. GOPINATH, R. W. BRIGGS, AND E. A. GEISER, *Using prior shapes in geometric active contours in a variational framework*, International Journal of Computer Vision, 50 (2002), pp. 315–328.
- [6] D. L. CHOPP, *Computing minimal surfaces via level set curvature flow*, University of California, Berkeley, 1991.
- [7] F. CLERICI, N. FERRO, S. MARCONI, S. MICHELETTI, E. NEGRELLO, AND S. PEROTTO, *Anisotropic adapted meshes for image segmentation: Application to three-dimensional medical data*, SIAM Journal on Imaging Sciences, 13 (2020), pp. 2189–2212.
- [8] V. ESTELLERS, D. ZOZZO, R. LAI, S. OSHER, J.-P. THIRAN, AND X. BRESSON, *Efficient algorithm for level set method preserving distance function*, IEEE Transactions on Image Processing, 21 (2012), pp. 4722–4734.
- [9] M. ETHIER AND Y. BOURGAULT, *Semi-implicit time-discretization schemes for the bidomain model*, SIAM Journal on Numerical Analysis, 46 (2008), pp. 2443–2468.
- [10] M. FALCONE, G. PAOLUCCI, AND S. TOZZA, *A high-order scheme for image segmentation via a modified level-set method*, SIAM Journal on Imaging Sciences, 13 (2020), pp. 497–534.
- [11] W. GAO AND A. BERTOZZI, *Level set based multispectral segmentation with corners*, SIAM Journal on Imaging Sciences, 4 (2011), pp. 597–617.
- [12] J. GOMES AND O. FAUGERAS, *Level sets and distance functions*, in Computer Vision-ECCV 2000: 6th European Conference on Computer Vision Dublin, Ireland, June 26–July 1, 2000 Proceedings, Part I

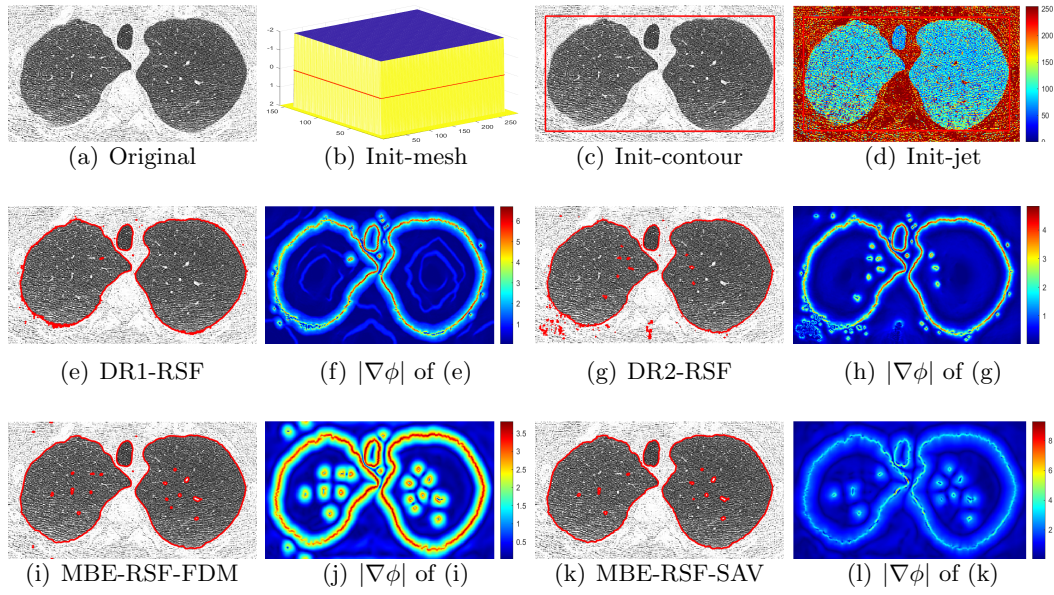


Figure 16. Segmentation results of DR1-RSF model, DR2-RSF model and MBE-RSF model.

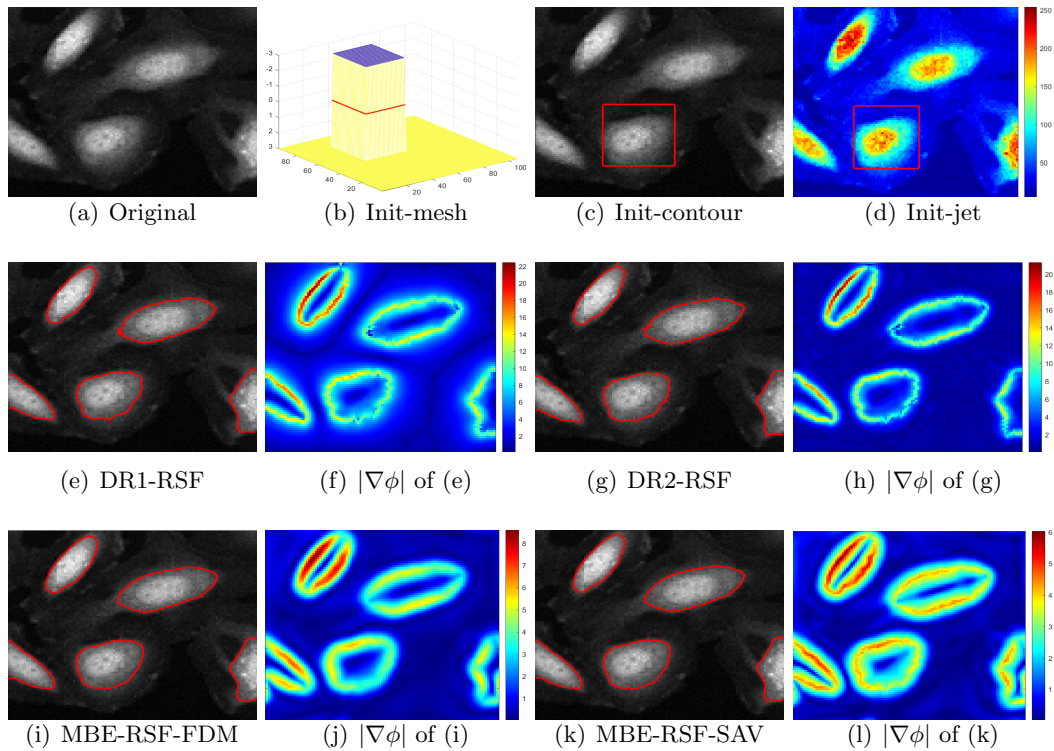


Figure 17. Segmentation results of DR1-RSF model, DR2-RSF model and MBE-RSF model.

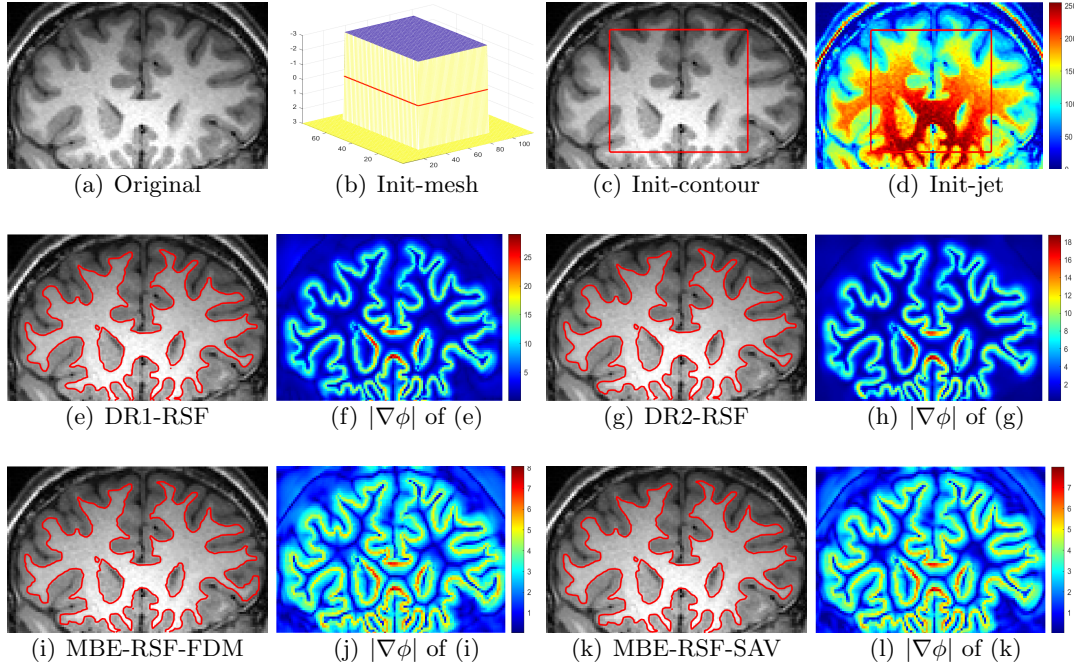


Figure 18. Segmentation results of DR1-RSF model, DR2-RSF model and MBE-RSF model.

- 6, Springer, 2000, pp. 588–602.
- [13] M. HEIDEMAN, D. JOHNSON, AND C. BURRUS, *Gauss and the history of the fast fourier transform*, IEEE Assp Magazine, 1 (1984), pp. 14–21.
- [14] J.-B. A. KAMGA AND B. DESPRÉS, *Cfl condition and boundary conditions for dgm approximation of convection-diffusion*, SIAM Journal on Numerical Analysis, 44 (2006), pp. 2245–2269.
- [15] B. LI AND J.-G. LIU, *Thin film epitaxy with or without slope selection*, European Journal of Applied Mathematics, 14 (2003), pp. 713–743.
- [16] B. LI, S. MA, AND K. SCHRATZ, *A semi-implicit exponential low-regularity integrator for the navier-stokes equations*, SIAM Journal on Numerical Analysis, 60 (2022), pp. 2273–2292.
- [17] C. LI, R. HUANG, Z. DING, J. C. GATENBY, D. N. METAXAS, AND J. C. GORE, *A level set method for image segmentation in the presence of intensity inhomogeneities with application to mri*, IEEE Transactions on Image Processing, 20 (2011), pp. 2007–2016.
- [18] C. LI, C.-Y. KAO, J. C. GORE, AND Z. DING, *Minimization of region-scalable fitting energy for image segmentation*, IEEE Transactions on Image Processing, 17 (2008), pp. 1940–1949.
- [19] C. LI, C. XU, C. GUI, AND M. D. FOX, *Level set evolution without re-initialization: a new variational formulation*, in 2005 IEEE Computer Society Conference on Computer Vision and Pattern Recognition (CVPR’05), vol. 1, IEEE, 2005, pp. 430–436.
- [20] C. LI, C. XU, C. GUI, AND M. D. FOX, *Distance regularized level set evolution and its application to image segmentation*, IEEE Transactions on Image Processing, 19 (2010), pp. 3243–3254.
- [21] D. LI, G. ZHANG, Z. WU, AND L. YI, *An edge embedded marker-based watershed algorithm for high spatial resolution remote sensing image segmentation*, IEEE Transactions on Image Processing, 19 (2010), pp. 2781–2787.
- [22] H. LI, W. GUO, J. LIU, L. CUI, AND D. XIE, *Image segmentation with adaptive spatial priors from joint registration*, SIAM Journal on Imaging Sciences, 15 (2022), pp. 1314–1344.
- [23] H. LI, W. GUO, J. LIU, L. CUI, AND D. XIE, *Image segmentation with adaptive spatial priors from joint registration*, SIAM J. Imaging Sci., 15 (2022), pp. 1314–1344, <https://doi.org/10.1137/21M1444874>.
- [24] C. LIU, Z. QIAO, AND Q. ZHANG, *Two-phase segmentation for intensity inhomogeneous images by the*

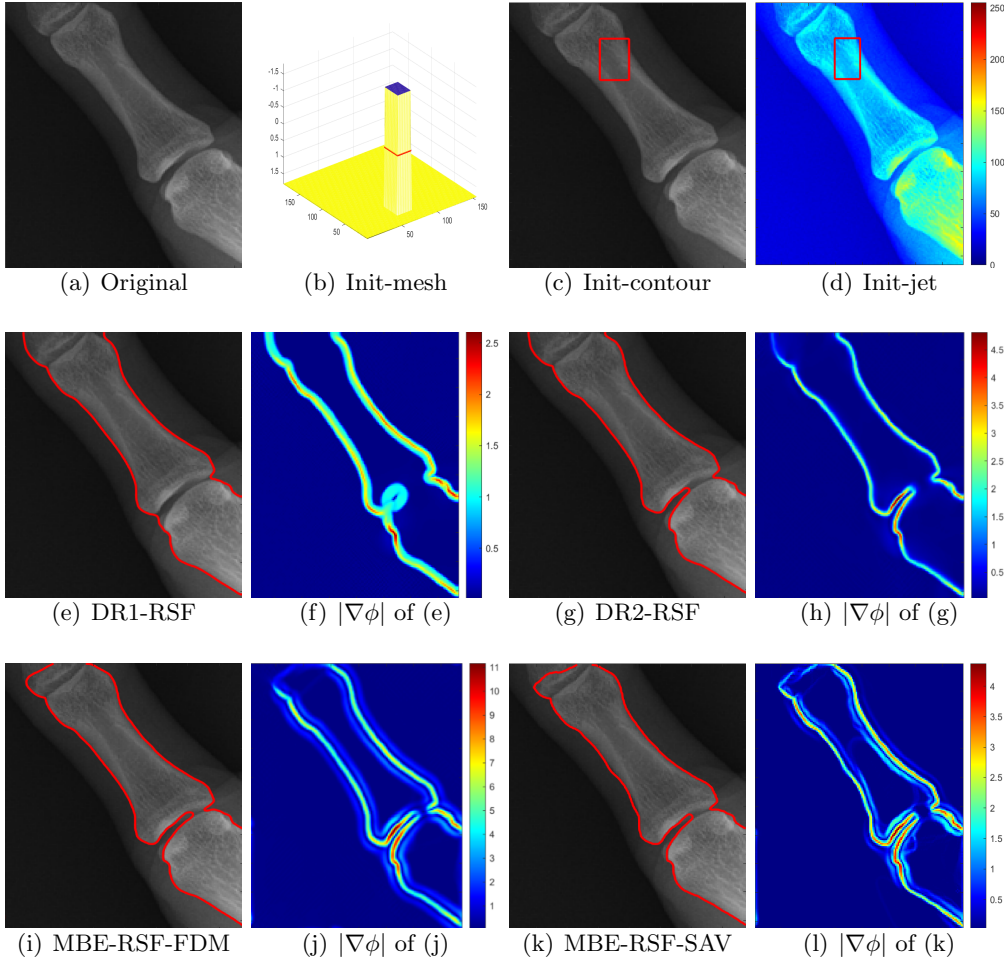


Figure 19. The segmentation results of DR1-RSF model, DR2-RSF model and MBE-RSF model.

allen–cahn local binary fitting model, SIAM Journal on Scientific Computing, 44 (2022), pp. B177–B196.

- [25] S. LUO, X.-C. TAI, AND R. GLOWINSKI, *Convex object(s) characterization and segmentation using level set function*, 64 (2022), pp. 68–88.
- [26] D. MOLDOVAN AND L. GOLUBOVIC, *Interfacial coarsening dynamics in epitaxial growth with slope selection*, Physical Review E, 61 (2000), p. 6190.
- [27] M. ORTIZ, E. REPETTO, AND H. SI, *A continuum model of kinetic roughening and coarsening in thin films*, Journal of the Mechanics and Physics of Solids, 47 (1999), pp. 697–730.
- [28] S. OSHER, R. FEDKIW, AND K. PIECHOR, *Level set methods and dynamic implicit surfaces*, Applied Mechanics Reviews, 57 (2004), pp. B15–B15.
- [29] S. OSHER AND J. A. SETHIAN, *Fronts propagating with curvature-dependent speed: Algorithms based on hamilton-jacobi formulations*, Journal of Computational Physics, 79 (1988), pp. 12–49.
- [30] N. OTSU, *A threshold selection method from gray-level histograms*, IEEE transactions on systems, man, and cybernetics, 9 (1979), pp. 62–66.
- [31] D. PENG, B. MERRIMAN, S. OSHER, H. ZHAO, AND M. KANG, *A pde-based fast local level set method*, Journal of Computational Physics, 155 (1999), pp. 410–438.
- [32] J. SHEN, J. XU, AND J. YANG, *A new class of efficient and robust energy stable schemes for gradient*

- flows*, SIAM Review, 61 (2019), pp. 474–506.
- [33] J. SHI AND J. MALIK, *Normalized cuts and image segmentation*, IEEE Transactions on Pattern Analysis and Machine Intelligence, 22 (2000), pp. 888–905.
- [34] M. SUSSMAN AND E. FATEMI, *An efficient, interface-preserving level set redistancing algorithm and its application to interfacial incompressible fluid flow*, SIAM Journal on Scientific Computing, 20 (1999), pp. 1165–1191.
- [35] L. VINCENT AND P. SOILLE, *Watersheds in digital spaces: an efficient algorithm based on immersion simulations*, IEEE Transactions on Pattern Analysis & Machine Intelligence, 13 (1991), pp. 583–598.
- [36] S. WALI, C. LI, M. IMRAN, A. SHAKOOR, AND A. BASIT, *Level-set evolution for medical image segmentation with alternating direction method of multipliers*, Signal Processing, 211 (2023), p. 109105.
- [37] E. W. WEISSTEIN, *Heaviside step function*, <https://mathworld.wolfram.com/>, (2002).
- [38] X. XIE, *Active contouring based on gradient vector interaction and constrained level set diffusion*, IEEE Transactions on Image Processing, 19 (2009), pp. 154–164.
- [39] W. YAO, J. SHEN, Z. GUO, J. SUN, AND B. WU, *A total fractional-order variation model for image super-resolution and its sav algorithm*, Journal of Scientific Computing, 82 (2020), pp. 1–18.
- [40] J. YUAN, E. BAE, AND X.-C. TAI, *A study on continuous max-flow and min-cut approaches*, in 2010 IEEE computer society conference on computer vision and pattern recognition, IEEE, 2010, pp. 2217–2224.
- [41] K. ZHANG, L. ZHANG, H. SONG, AND D. ZHANG, *Reinitialization-free level set evolution via reaction diffusion*, IEEE Transactions on Image Processing, 22 (2012), pp. 258–271.
- [42] W. ZHANG, X. WANG, W. YOU, J. CHEN, P. DAI, AND P. ZHANG, *RESLS: region and edge synergetic level set framework for image segmentation*, 29 (2020), pp. 57–71.
- [43] H. ZHAO, *A fast sweeping method for eikonal equations*, Mathematics of Computation, 74 (2005), pp. 603–627.